FLOW IN RECTANGULAR MICROCHANNELS: AN EXPERIMENTAL INVESTIGATION

M. Akbari*
Department of Mechanical Engineering,
University of Victoria, Victoria, BC, Canada, V8W 2Y2.
M. Bahrami†
Mechatronic System Engineering, School of Engineering science,
Simone Fraser University, Surrey, BC, Canada, V3T 0A3.
D. Sinton‡
Department of Mechanical Engineering,
University of Victoria, Victoria, BC, Canada, V8W 2Y2.

Pressure driven liquid flow through rectangular cross-section microchannels was investigated in this work. Microchannels fabricated using soflt lithography method on PDMS/PDMS substrates. Pressure drop data are used to characterize the friction factor for the wide channel aspect ratios in the range 0.13–0.76 and over a Reynolds number range 1– 45. Distilled water were used in this study as working fluid. Comparison with conventional model and previous works revealed that distinguishable deviation from Stokes flow theory was not observed for any channel cross-section.

Nomenclature

a	=	radius, m
A_c	=	micro channel cross-section area, m^2
A_t	=	tubing cross-section area, m^2
f	=	Fanning friction factor, $-$
H	=	microchannel half height, m
I_p	=	polar momentum of inertia, m^4
I_p^*	=	specific polar momentum of inertia, I_p/A_c^2, $-$
K_{bend}	=	loss coefficient for bend, $-$
K_c	=	contraction loss coefficient, $-$
K_e	=	expansion loss coefficient, $-$
L	=	microchannel length, m
L_{in}	=	flow developing region length, m
Po	=	Poiseuille number, $f\,\mathrm{Re}_{\sqrt{A_c}}$
Q	=	volumetric flow rate, m^3/s
$\mathrm{Re}_{\sqrt{A_c}}$	=	Reynolds number, $\rho Q/\mu\sqrt{A_c}$

Greek

ε	=	aspect ratio, $2H/2W$, $-$
Γ	=	cross-section perimeter, m
μ	=	fluid viscosity, $kg/m.s$
μ_a	=	apparent viscosity, $kg/m.s$
μ_{eo}	=	electroosmotic mobility, $m^2/V.s$
ρ	=	fluid density, kg/m^3
σ_b	=	fluid electrical conductivity, S/m
ω_f	=	friction factor uncertainty, $-$

INTRODUCTION

Advances in microfabrication make it possible to build microchannels with small dimensions, in order of micrometers. Micro- and minichannels show promising potential and have been incorporated in a wide variety of unique, compact, and efficient cooling applications such as in microelectronic devices. These micro heat exchangers or heat sinks feature [1] extremely high heat transfer surface area per unit volume ratios, high heat transfer coefficients, and low thermal resistances . In biological and life sciences, microchannels are used widely for analyzing biological materials such as proteins, DNA, cells, embryos and chemical reagents [2]. Various microsystems such as micro-heat sinks, micro-biochips, micro-reactors and micronozzles have been developed in recent years [3–6]. Since microchannels are usually integrated in these microsystems, it is important to determine the characteristics of the fluid flow in microchannels for better design of various microflow devices.

In parallel to the recent attentions to microfluidic devices, microfabrication techniques have also evolved significantly. Some of the important fabrication techniques include lithography (soft and photolithography), lamination, injection molding, hot embossing, micromachining with laser, and electrochemical or ultrasonic technologies [7]. Together with new methods of fabrication, it is possible to exploit certain fundamental differences between the physical properties of fluids moving in large channels and those travelling through micrometer-scale channels [2]. Different cross-sections such as rectangular, circular, trapezoidal,

*PhD Candidate and Corresponding author. E-mail: makbari@uvic.ca. Tel: +1 (250)884-7339
†Assistant Professor. Email: mbahrami@sfu.ca
‡Assistant Professor.Email: dsinton@uvic.ca

triangular, and elliptical were investigated by several researchers to understand the flow behavior in microchannels. Rectangular and trapezoidal cross-sections have been extensively studied for a wide range of applications, mainly due to practical considerations such as fabrication techniques, cost, ease of manufacturing [7]. Most researchers employed rectangular cross-sections for studying friction and pressure drop in microchannels [8–11]. Since microchannels length is normally long (compared to other dimensions), inlet and exit effects have been neglected in most works.

In recent years, a large number of papers have reported pressure drop data for laminar fully developed flow of liquids in microchannels with various cross-sections. However, published results are often inconsistent. Tuckerman and Pease [12] employed rectangular microchannels as high-performance heat sinks for cooling electronic components. They found that the experimental results of flow friction were slightly higher than those predicted by classical theories. Peng et al. [8] experimentally studied the flow and heat transfer characteristics of water flow through rectangular cross-section microchannels with hydraulic diameters ranging from 130 μm to 340 μm. They [8] used precision machining microfabrication method on stainless steel substrates. Significant deviation from the characteristics of the macro-size channel flow was observed in their work. This deviation was attributed to an early onset of laminar to turbulent flow transition. Same results and discussion were reported by Xu et. al. [9] and Mala and Li [13]. Pfhaler et al. [14] and [15], Urbanek et al. [16], Qu et al. [17], Papautsky et al. [18], Ren et al. [10] and [19], Weilin et. al. [20] and Guo and Li [21] explained that deviations would originate from surface phenomena such as surface roughness, electrokinetic forces, temperature effects and microcirculation near the wall. Ren et al. [10] and [19] provided a comprehensive study on electroviscous effect in microchannels. They demonstrated that electroviscous effect on the pressure drop strongly depends on the channel dimensions and ionic concentration of the working liquid. Bahrami et al. [22] proposed an analytical model to predict the pressure drop in fully developed laminar flows in rough microtubes. They showed that the effect of roughness is to increase the pressure drop in microtubes. and can be neglected when the relative roughness is less than 3%.

Jiang et al. [23], conducted an experimental investigation of water flow through different shapes of microchannel cross section including circular, rectangular, trapezoidal and triangular. The hydraulic diameter of microchannels varied from 8 μm to 42 μm. They collected experimental data with the Reynolds number ranging from 0.1 to 2, and concluded that there was less influence of the cross-sectional shape on the microflow in the microchannel and the experiment data agreed well with the prediction of the convention theory. Baviere et. al. [24], performed an experimental study on the water flow through smooth rectangular microchannels. Their channels were made of a silicon engraved substrate anodically bonded to a Pyrex cover. Their results showed that in smooth microchannels, the friction law is correctly predicted by conventional theories. Judy et. al. [11] and Bucci et. al. [25] showed that their experimental results were in good agreement with conventional theories, in laminar regime. Also Wu and Cheng [26], Lio and Garimella [27] and Gao et al. [28] reported good agreement between experimental data with conventional theories.

Recently, discrepancies among the work of many researchers have been summarized in a review paper by Steinke and Kandlikar [29]. Interestingly, it was reported that the deviations are higher at lower Reynolds numbers. They listed developing region effect, inlet, exit and other minor losses and uncertainty in the measurements as the reasons for the observed deviations from the classical models in the literature.

The contradictions among different researches indicate that the flow in microchannels are still needed to be well understood. The objectives of present work are: 1) to experimentally investigate the characteristics of single-phase liquid flow in microchannels, and 2) resolve some of the disagreements observed in the existing data. We focus on a comprehensive experimental investigation of liquid flow with an emphasis on careful measurements. Low Reynolds numbers have been studied in this work. Rectangular cross-section microchannels with a range of aspect ratios were fabricated using soft lithography method on PDMS/PDMS substrates**.** Efforts have been made to investigate the effects of developing region pressure drop, minor losses, streaming potential on the pressure drop in details.Viscous dissipation and roughness effects are neglected in this study. Further, the experimental data are compared to the model proposed by Bahrami et al. [1], and also data collected by others. Based on the experimental results, attempts have been made to show that the conventional theory is applicable in microscales.

THEORETICAL MODELING

The low Reynolds number flow regime is one of the characteristic of flows in microchannels [30]. Hence, nonlinear terms in Navier-Stokes equation disappear, resulting in the Poisson's equation

$$\nabla^2 u = \frac{1}{\mu}\frac{dP}{dz} \quad \text{with } u = 0 \text{ on } \Gamma \tag{1}$$

where u is the fluid velocity, z is the flow direction and Γ is the perimeter of the channel. Equation (1) is applicable of fully developed flow. Exact solution for Eq. (1) in rectangular cross-section channels can be found in fluid mechanics textbooks such as White [31]. The original analytical solution for the mean velocity in rectangular channels is in the form of a series, but it has been shown [1] that using the first term of the series results in errors less than 0.7%. Shah and London [32] eported a correlation for determining the Poiseuille number in rectangular channels as a function of channel aspect ratio.

Bahrami et al. [1,33], developed a general model for prediction of pressure drop in microchannels of arbitrary cross-

section. Using the analytical solution of elliptical duct and the concept of Saint-Venant principal in torsion [34], they showed that the Poiseuille number, $f\,\mathrm{Re}_{\sqrt{A_c}}$, is a function of the polar moment of inertia, I_p, area, A_c, and perimeter of the cross-section of the channel, Γ. Their model showed good agreement with experimental and numerical data for a wide variety of cross-sections such as: rectangular, trapezoidal, triangular, circular, and moon shaped. The objective of this paper is to first investigate the accuracy of their model; and later on extend it to more general geometries such as converging and diverging microchannels.

Selection of the characteristic length is an arbitrary choice and will not affect the final solution. However, an appropriate length scale leads to more consistent results, especially when general cross-section is considered. A circular duct is fully described with its diameter, thus the obvious length scale is the diameter (or radius). For non-circular cross-sections, the selection is not as clear; many textbooks and researchers have conventionally chosen the hydraulic diameter, as the characteristic length. Yovanovich [35, 36] introduced the square root of area as a characteristic length scale for heat conduction and convection problems. Later, Muzychka and Yovanovich [37] proposed the use of $\sqrt{A_c}$ for the fully-developed flow in non-circular ducts. Bahrami et al. [1, 33] showed through analysis that square root of area appears in the solution of fully-developed flow in non-circular ducts. They also compared both D_h and $\sqrt{A_c}$ and observed that using $\sqrt{A_c}$ as the characteristic length scale results in similar trends in Poiseuille number for microchannels with a wide variety of cross-sections. Therefore, in this study, $\sqrt{A_c}$ is selected consistently as the length scale throughout the analysis.

According to this model Poiseuille number in this model can be obtained from [1]

$$Po = f\,\mathrm{Re}_{\sqrt{A_c}} = 32\pi^2 I_p^* \frac{\sqrt{A_c}}{\Gamma} \tag{2}$$

where

$$\mathrm{Re}_{\sqrt{A_c}} = \frac{\rho Q}{\mu\sqrt{A_c}} \tag{3}$$

Note that the square root of the microchannel cross section, $\sqrt{A_c}$ was used as the characteristic length in Eq. (3).Based on Bahrami et al. model [1], the Poiseuille number is only a function of geometrical parameters of the channels. Relationships for various geometries have been provided in [1]. Substituting for geometrical parameters in Eq. (2) for rectangular cross-section channels, Poiseuille number can be found to be only a function of microchannel aspect ratio, ε [1]

$$f\,\mathrm{Re}_{\sqrt{A_c}} = \frac{4\pi^2\left(1+\varepsilon^2\right)}{3\sqrt{\varepsilon}\,(1+\varepsilon)} \tag{4}$$

where $\varepsilon = 2H/2W$.

EXPERIMENTAL

Chemicals and materials

De-ionized water has been used as the testing liquid. The fluid properties are $\rho = 998\ kg/m^3$ and $\mu = 0.001\ kg/(m.s)$ and constant. We assumed that the viscous heating effect is negligible for the range of Reynolds number investigated in this work. SU-8 photoresist (Microchem, Newton, Massachusetts, USA) and Diacetone-alcohol developer solution (Sigma-Aldrich, St.Louis, Missouri, USA) were used in the making of the positive relief masters by the procedure outlined below. PDMS casts were prepared by thoroughly mixing the base and curing agent at a 10:1 ratio as per the manufacturers instructions for the Sylgard 184 silicon elastomer kit (Dow Corning, Midland, Michigan, USA). Caution was used to avoid contact between the liquid PDMS and latex rubber (gloves) as this was found to inhibit curing [38].

Microfabrication

The PDMS/PDMS microchannels used in this study have been manufactured using the soft lithography technique described by Erickson et. al. [38] (Fig. 1). Briefly, photomasks needed are designed by AutoCAD software (www.usa.autodesk.com) and printed by a 3500 DPI printer (Island graphics Ltd., Victoria, BC). Masters containing the desired microchannel pattern have been made by spin coating SU-8 negative photoresist on a glass slide to a nominal desired thickness. The photoresist film was then hardened through a two-stage direct contact pre-exposure bake procedure (65 °C for 15 min and 95 °C for 30 min) and exposed to UV light for 100 sec through the mask containing the channel pattern. A two stage post-exposure bake procedure (65 °C for 1-2 min. 95 °C for 20 min.) was then used to enhance cross-linking in the exposed portion of the film. The slide was then placed in quiescent developer solution for 10 min. to dissolve the unexposed photoresist, leaving a positive relief containing the microchannel pattern.

Liquid PDMS was then poured over the master and exposed to vacuum condition (1 hr) to exrtact all the bubbles in it. Then cured at 85 °C for 15-20 min yielding a negative cast of the microchannel pattern. An enclosed microchannel was then formed by bonding the PDMS cast with either another piece of PDMS with plasma treating. All above procedure was carried out under a clean condition to avoid any impurities effecting the fabrication process.

Five microchannels were made with a range of aspect ratios, $0.13 < \varepsilon = 2H/2W < 0.76$, and tested in this study. Dimensions of the microchannels are shown in Table 1. Since channel dimensions have a major effect on the friction factor calculations [9], [11] and [29], a destructive careful measurement was performed after the experiments. Channels were cut at three random cross-sections and dimensions of the channel were measured by an image processing method. To do so, a Leica DMI 6000B

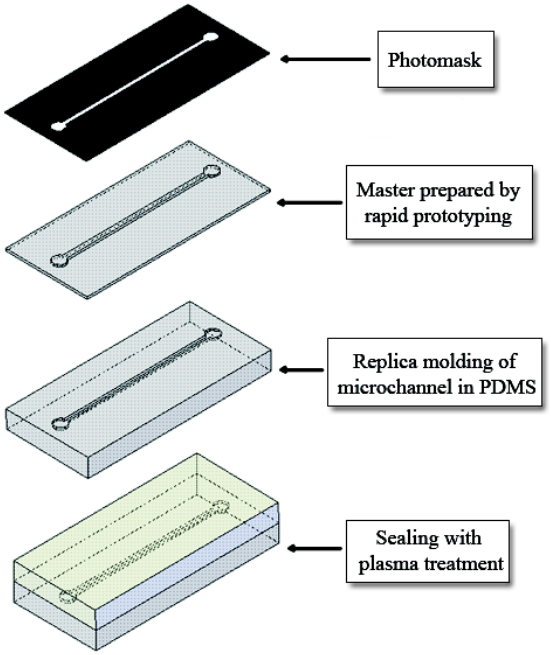

Fig. 1 Schematic of soft lithography technique.

(Leica microsystems, RichmondHill, Ontario, Canada) microscope with a 10×, 0.4 N.A. objective was used. Images of the channel cross-section were captured by a high resolution, high sensitivity CCD (Hamamatsu Orca AG) and imported in a photo edit software, Adobe Photoshop 8.0 (www.adobe.com). Dimensions of the channel were then measured by pixel counting. Size of each pixel was calibrated by a known dimension, then number of pixels in the width or height of the channel were counted to find the dimensions of the channel. Figure 2 shows the microchannel cross-section taken for the specie PPR-0.17, typically. As can be seen, due to fabrication process, microchannel cross-section has an arbitrary shape, but it is close to rectangle. Height and width measurements were conducted at different positions for each cross-section and the average value was considered. This measurement was also performed at several cross-sections. Mean values are reported in Table 1. It was observed that both microchannel depth and width were different from the expected values in the fabrication process. From our measurements, channel height changed less than 4% and its width changed less than 3% with respect to spin coating procedure prediction and mask size during the fabrication.

Experimental procedure

An open loop syringe pump system, as illustrated in Figure 3 was chosen for this work. A syringe pump (Harvard Apparatus, Quebec, Canada) provided constant flow rate with ±0.5% accuracy. A range of Reynolds number was covered by changing the volumetric flow rate from $40\mu L/\min$ to 240 $\mu L/\min$. Reynolds number was calculated using Eq. (3), having the volumetric flow rate, Q. To prevent entering bubbles into the transducer a 0.2 μm

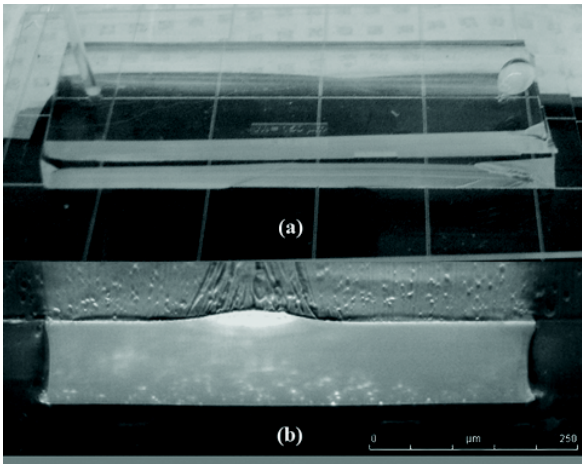

Fig. 2 (a) Microchannel under the test and (b) microchannel cross-section (image taken by Leica 6000DMI-B microscope), channel # PPR-0.17.

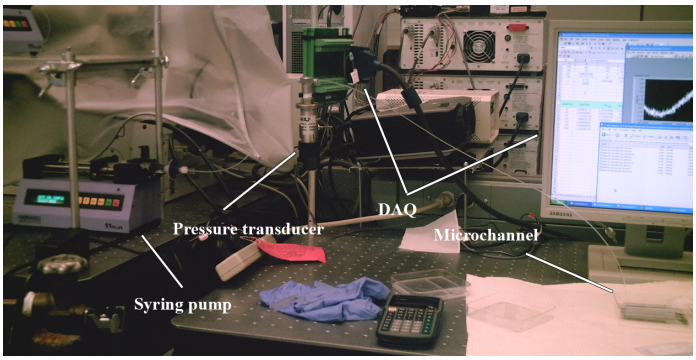

Fig. 3 Microchannel pressure mearusment test section.

filter (Aktreingeselchaf Co., Germany) was installed after the pump. Water was forced to flow through this submicron filter before entering the channel. Droplet formed during the test at the channel outlet was collected repeatedly to avoid its surface tension effect on our measurments. To measure the pressure drop, a gauge pressure transducer (Omega Inc., Laval) was fixed at the channel inlet while the channel outlet was opened to the atmosphere. Teflon tubing (Scientific products & equipment, Noth York, ON, Canada) was employed to connect pressure transducer to the syringe pump and the microchannel. Values of measured pressure were then monitored and recorded with a computerized data acquisition system (Labview 8.5, National Instrument, www.ni.com). The flow was considered to have reached a steady state condition when the readings of the pressure drop did not change any more. The data reported in this paper are for steady state flow. For a given channel, the measurement of pressure drop were repeated three times for each flow rate. Each measurement started when the transducer showed zero pressure. An arithmetic averaging method [39] was performed to determine the final results.

Table 1 Ratio of developing pressure drop to measured pressure drop of the channel

Channel	Width, $2W$ $[\mu m]$	Depth, $2H$ $[\mu m]$	Length, L $[mm]$	$\sqrt{A_c}$ $[\mu m]$	$\varepsilon = H/W$	$\sqrt{A_c}/L$
$PPR-0.13$	780	110	50.0	293.0	0.13	0.006
$PPR-0.17$	581	101	50.0	242.0	0.17	0.005
$PPR-0.40$	480	192	58.8	303.6	0.40	0.005
$PPR-0.60$	189	113	55.5	146.4	0.60	0.003
$PPR-0.76$	134	103	50.0	117.3	0.76	0.002

RESULTS AND DISCUSSION

Total measured pressure drop during the experiment, $\Delta P_{measured}$ is

$$\begin{aligned}\Delta P_{measured} &= \Delta P_c+\Delta P_{con}+\Delta P_D+\Delta P_{FD} \\ &\quad +\Delta P_{ex}+2\Delta P_b+\Delta P_{ev}\end{aligned} \tag{5}$$

where ΔP_c is the pressure loss due to the flow in the connecting tubes, ΔP_{con} and ΔP_{ex} are the inlet and exit losses, ΔP_D is the developing region loss, ΔP_{FD} is the pressure drop in the fully developed region, ΔP_b is the pressure drop due to 90 degrees bends and ΔP_{ev} is pressure drop corresponds to electroviscous effect. Since fully developed pressure drop is the focus of this study, right hand side losses except ΔP_{FD} should be subtracted from the measured pressure drop.

Connecting tube pressure loss, ΔP_c The connecting tube pressure drop includes the losses due to all fittings and the capillary tube from the transducer to the microchannel inlet. We measured this loss directly at each flow rate when there was no microchannel at the end of the tubing. The measurements were carefully conducted and all conditions were identical to the case which microchannel was at the end of the connecting tube.

Developing region, ΔP_D Since the viscous boundary layer inherently grow faster in microchannels than in macroscales, the developing region in most cases is negligible. There are few references can be found in the literature in which the effect of inlet region was considered [40], [41] and [32].Phillips [40] showed that the length of the hydrodynamic developing region, L_{in}, depends on the aspect ratio of rectangular cross-section microchannels, the higher aspect ratio, the longer developing length. Maximum value of L_{in} can be obtained from Eq. (6):

$$L_{in} = \left(\frac{16A_c\sqrt{A_c}}{\Gamma^2}\right)\mathrm{Re}_{\sqrt{A_c}} \tag{6}$$

Pressure drop of the entrance region is then [40]

$$\Delta P_D = \frac{8\left(f\,\mathrm{Re}_{\sqrt{A_c}}\right)\mu Q\sqrt{A_c}}{\Gamma D_h^2}L_{in} + K\frac{\rho Q^2}{2A_c^2} \tag{7}$$

In this equation K is a constant and related to the microchannel aspect ratio as follows

$$\begin{aligned}K &= 0.6796 + 1.2197\varepsilon + 3.3089\varepsilon^2 \\ &\quad -9.5921\varepsilon^3 + 8.9089\varepsilon^4 - 2.9959\varepsilon^5\end{aligned} \tag{8}$$

In Eq. (7), $f\,\mathrm{Re}_{\sqrt{A_c}}$ was calculated based on the measured pressure drop, in this work. Table 2 lists the relative pressure loss of developing region with respect to the measured pressure drop, in percent. As can be seen, the values are small, less than 0.3%, thus can be neglected for the range of Reynolds number studied in this work ($1 < \mathrm{Re}_{\sqrt{A_c}} < 35$). For higher Reynolds numbers ($\mathrm{Re} \sim 100$), developing pressure drop, ΔP_D was found to be less than 2% of the fully developed pressure drop obtained from Eq. (4).

Minor losses, $\Delta P_{\mathrm{min\,or}}$ Other pressure losses associated with the measured pressure drop are entrance, exit and bend losses. These losses are usually obtained from the traditional relationships used in macroscale [11], [29], [40], [42]. Phillips [40] showed that the minor pressure losses can be obtained from Eq. (9)

$$\begin{aligned}\Delta P_{\mathrm{min\,or}} &= \Delta P_{in} + \Delta P_{exit} + 2\Delta P_b = \\ &\quad \frac{\rho Q^2}{2A_c^2}\left[K_c + K_e + 2K_{bend}\left(\frac{A_c}{A_t}\right)^2\right]\end{aligned} \tag{9}$$

where A_c and A_t are the channel and tubing cross-sectional areas, respectively, K_{bend} is the loss coefficient for the bend and K_c and K_e represent the contraction and expansion loss coefficients due to area changes. Phillips [40] recommends K_{bend} to be approximately 1.2 for a 90 degree bend. Assuming equal cross-sectional areas for the channel and tubing and also maximum possible values for K_c and K_e [43] relative minor losses with respect to the measured pressure drop, in percent, are listed in Table 3. As can be seen, these losses are negligible compared to the measured pressure drop. For higher Reynolds numbers ($\mathrm{Re} \sim 100$), developing pressure drop, $\Delta P_{\mathrm{min}\,or}$ was found to be less than 5% of the fully developed pressure drop obtained from Eq. (4).

Electroviscous effect, ΔP_{ev} When a liquid is forced through a narrow channel under an applied pressure gradient, the counterinons in the diffusive layer of EDL are moving towards the down stream end and a potential gradient is induced in the flow [45]. This so called *streaming*

Table 2 Percentage of developing region pressure drop to measured pressure drop of the channel

$\Delta P_D/\Delta P_{measured}[\%]$					
$Q\left[\frac{\mu L}{\min}\right]$	$\varepsilon=0.13$	$\varepsilon=0.17$	$\varepsilon=0.40$	$\varepsilon=0.60$	$\varepsilon=0.76$
40	0.01	0.01	0.04	0.03	0.04
60	0.01	0.02	0.03	0.04	0.06
80	0.01	0.02	0.04	0.06	0.08
100	0.02	0.01	0.06	0.07	0.10
120	0.02	0.02	0.06	0.08	0.11
240	0.03	0.05	0.10	0.20	0.24

Table 3 Percentage of minor pressure losses to measured pressure drop of the channel

$\Delta P_{\min or}/\Delta P_{measured}[\%]$					
$Q\left[\frac{\mu L}{\min}\right]$	$\varepsilon=0.13$	$\varepsilon=0.17$	$\varepsilon=0.40$	$\varepsilon=0.60$	$\varepsilon=0.76$
40	0.04	0.04	0.12	0.09	0.11
60	0.05	0.07	0.10	0.13	0.17
80	0.07	0.10	0.14	0.17	0.23
100	0.08	0.07	0.21	0.22	0.28
120	0.09	0.10	0.19	0.25	0.35
240	0.16	0.24	0.35	0.51	0.70

potential acts to drive the counterions in the diffuse layer of the EDL to move in the direction opposite to the pressure driven flow. The overall result is a reduced flow rate for a constant pressure gradient or increased in pressure drop for a given flow rate. This phenomena which gives the appearance of an increased viscosity, μ_a, is called *electroviscous effect* [45]. The ratio of this apparent viscosity to the fluid viscosity can be found from Eq. (10) for circular cross-section capillaries [46]

$$\frac{\mu_a}{\mu} \simeq 1 + \frac{32\mu}{\sigma_b a^2}\mu_{eo}^2 \tag{10}$$

where μ is the fluid viscosity, σ_b is the liquid electrical conductivity and a is the radius of capillary. $\mu_{eo} = \epsilon_0\epsilon_r\zeta/\mu$ is called electroosmotic mobility where $\epsilon_0 = 8.854 \times 10^{-12}$ $C^2V^{-1}m^{-1}$ is the permittivity of vacuum, $\epsilon_r = 78.3$ is the relative permittivity for water at $25°C$ [45] and ζ is the zeta potential of the surface. Approximating the rectangular cross-section microchannel with a capillary of the same hydraulic diameter, $\sigma_b = 5.6 \times 10^{-6} Sm^{-1}$ [47] and $\mu_{eo} = 5.9 \times 10^{-8} m^2V^{-1}s^{-1}$ [48] for PDMS, variation of μ_a/μ with respect to hydraulic diameter is plotted in Fig. 4. As can be seen, for small hydraulic diameters, $D_h < 100$ μm , the apparent viscosity becomes important. Consistent with the work of Ren and Li [10], for larger channel sizes, the apparent viscosity is very close to the actual viscosity of the liquid and streaming potential effect is not significant. In this work, since minimum hydraulic diameter is 116.2 μm electroviscous effect was neglected.

Uncertainty analysis A careful analysis of the experimental uncertainty in this study is critical to the interpretation of experimental data of friction factor, f and exploration of deviation from macroscale theory. Neglecting developing region and minor losses and also electroviscous effect, the fully developed pressure drop is

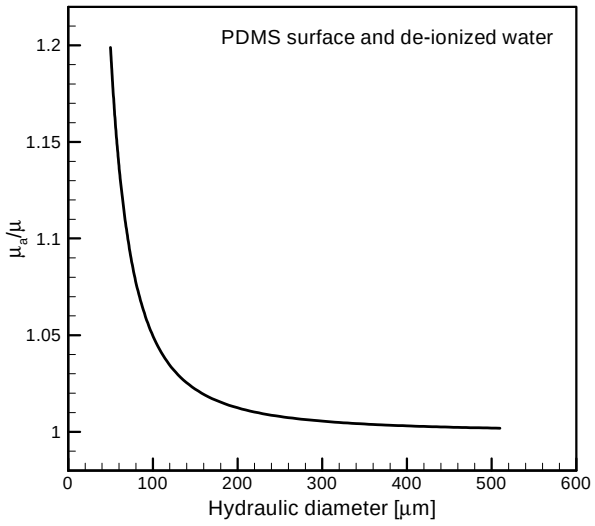

Fig. 4 Variation of the ratio of apparant viscosity to fluid viscosity.

$$\Delta P_{FD} = \Delta P_{measured} - \Delta P_c \tag{11}$$

Then the experimental fanning friction factor can be obtained from

$$f_{\exp} = \frac{\Delta P_{FD}}{2L}\left(\frac{D_h A_c^2}{\rho Q^2}\right) \tag{12}$$

Table 4 Uncertainty values in measured parameters.

Parameter	Maximum uncertainty [%]
$\Delta P_{measured}$	± 0.25
L	± 0.01
D_h	± 6.12
A_c	± 4.42
Q	± 0.5

The uncertainty in the friction factor, f, based upon the measured variables is given by [39]

$$\omega_f = \sqrt{\sum_{i=1}^{n} \left(\frac{\partial f}{\partial x_i} \omega_i \right)^2} \tag{13}$$

where x_i is a variable used to calculate the friction factor, f and ω_i is the corresponding uncertainty. Since friction factor takes the form of a product of the measured variables it is beneficial to study the relative friction factor uncertainty

$$\frac{\omega_f}{f} = \left[\begin{array}{c} \left(\frac{\omega_{\Delta P}}{\Delta P} \right)^2 + \left(\frac{\omega_L}{L} \right)^2 + \left(\frac{\omega_{D_h}}{D_h} \right)^2 + \\ \left(\frac{2\omega_{A_c}}{A_c} \right)^2 + \left(\frac{\omega_Q}{Q} \right)^2 + \left(\frac{\omega_\rho}{\rho} \right)^2 \end{array} \right]^{1/2} \tag{14}$$

From Eq. (14), it can be seen that the channel dimensions plays an important role in determination of uncertainty. Also for small Reynolds numbers, the accuracy of the flow rate becomes more significant. Maximum uncertainty in the measurement of measured variables is listed in Table 4.

Note that channel cross-section and hydraulic diameter uncertainty was obtained from the measured parameters, channel width, $2W$, and depth, $2H$, using the same method described. Uncertainty associated with this experiment was calculated to be less than 10%.

Figures 5 and 6 show the comparison between friction factor obtained from Eq. (4), solid line, and experimental data for channels PPR-0.13 and PPR-0.76, respectively. As shown the trend and values of experimental data are similar to that of predicted by Bahrami et al. model.

Variation of the Poisueille number, $f\,\mathrm{Re}_{\sqrt{A_c}}$, with the Reynolds number for different channels is shown in Fig. 7. Experimental data is normalized by analytical data obtained from Eq. (4). The solid line shows the analytical model. From Eq. (4), it is obvious that the frictional resistance, $f\,\mathrm{Re}_{\sqrt{A_c}}$, does not depend on the Reynolds number. Same trend can be observed from the experimental data. As can be seen most of the experimental points fell within $\pm 10\%$ bounds of the analytical model.

Another comparison of present experimental work with analytical model of Bahrami et al. is illustrated in Fig. 8.

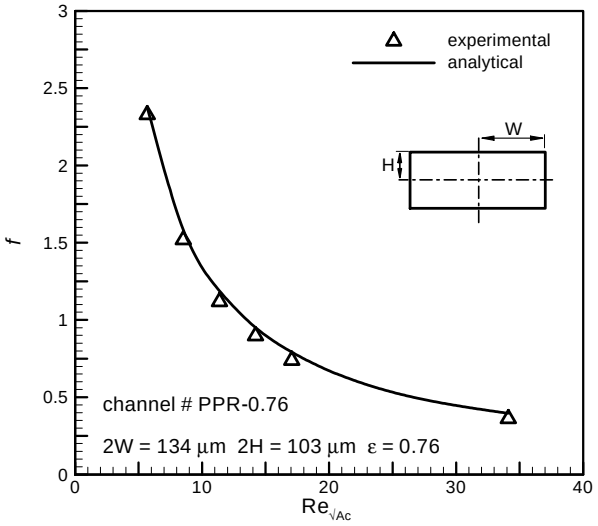

Fig. 5 Variation of friction factor with the Reynolds number, $\varepsilon = 0.13$.

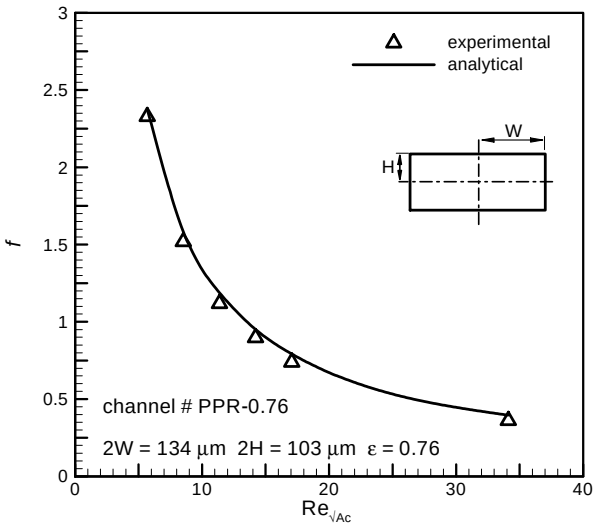

Fig. 6 Variation of friction factor with the Reynolds number, $\varepsilon = 0.76$.

Since Poisueille number, $f\,\mathrm{Re}_{\sqrt{A_c}}$ remains constant for the laminar regime as the Reynolds number varies, the experimental data for each set were averaged over the laminar region. The $\pm 10\%$ bounds of the model are also shown in the plot, to better demonstrate the agreement between the data and the model, Eq. (4).

As can be seen in Eq.(4), Poisueuille number, $f\,\mathrm{Re}_{\sqrt{A_c}}$, is only a function of the aspect ratio, $\varepsilon = H/W$, which is a geometrical parameter. This dependency is plotted in Fig. 9. Averaged values of different Reynolds number were used in this plot. Experimental data from present work

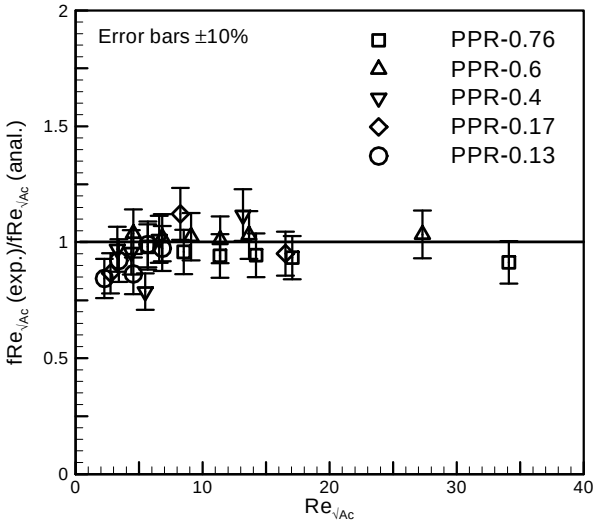

Fig. 7 Variation of Poisueuille number, $f\,\mathrm{Re}_{\sqrt{A_c}}$ with the Reynolds number.

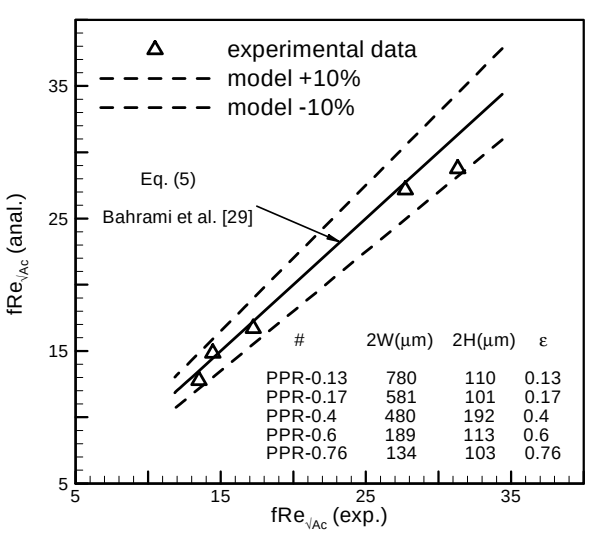

Fig. 8 Comparison of experimental data of present work with analytical model of Bahrami et. al. (2006).

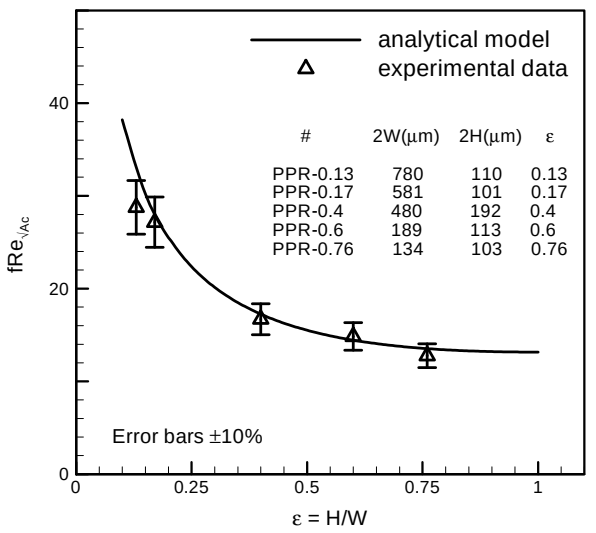

Fig. 9 Variation of Poiseuille number, $f\,\mathrm{Re}_{\sqrt{A_c}}$,with the channel aspect ratio.

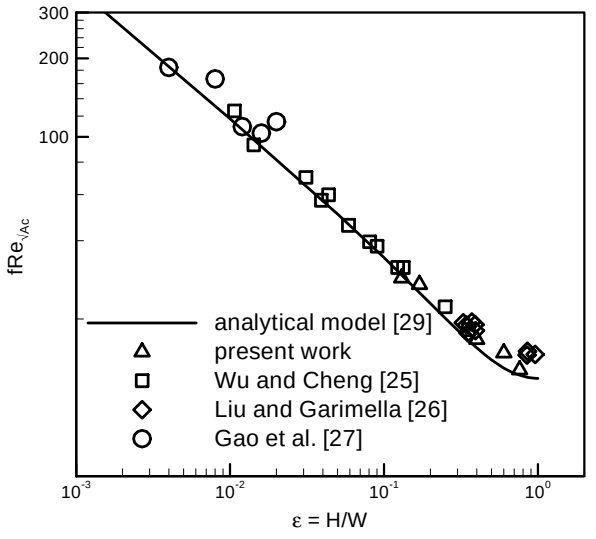

Fig. 10 Comparison between experimental data of present study and previous works.

captures the trend and values of analytical model with good agreement. It can be observed that for smaller aspect ratios frictional resistance , $f\,\mathrm{Re}_{\sqrt{A_c}}$, increases sharply.

It is beneficial to compare the results of present work with the existing data of rectangular microchannels. Data was collected from the works of Wu and Cheng [26], Lu and Garimella [27] and Gao et al. [28]. As shown in Fig. 10, the collected data cover a wide range of the aspect ratio, $\varepsilon = 2W/2H$, almost three decades. Solid line represents the analytical model of Bahrami et al. [1]. The relative difference between present data, analytical model and results of previous works is within the uncertainty of the experiments.

SUMMARY AND CONCLUSIONS

Frictional pressure drop measurements have been made over a range of Reynolds number for rectangular cross-section microchannels fabricated with soft lithography method in the aspect ratio range, $0.13 < \varepsilon < 0.76$. A careful measurement of pressure drop as well as calculations of developing region, minor losses and pressure drop due to electroviscous effect revealed that conventional theories

are still applicable in microscales with good accuracy. Uncertainty analysis showed that the measurement of channel dimensions and flow rate is critical in microscales. Hence, processing of the high quality images of the channel cross-section was conducted to find out the size of the microchannel. It is concluded that for the range of the microchannel explored in this study any non-stokes flow effect is at the level within the experimental uncertainty.

ACKNOWLEDGMENT

The authors gratefully acknowledge the financial support of the the Natural Sciences and Engineering Research Council of Canada, NSERC. Also our thanks go to Dr. Viatcheslav Berejnov and Mr. Ali K. Oskooi for their helps and supports.

References

[1] Bahrami, M., Yovanovich, M.M., Culham, J.R., 2006, Pressure drop of laminar, fully developed flow in microchannels of arbitrary cross-section, ASME Journal of Fluids Engineering 126, 1036-1044.

[2] Whitesides, G.M, 2006, The origins and the future of microfluidics, Nature 442, 368-372.

[3] Grushka, E., McCormick, R.M., Kirkland, J.J., 1989, Effect of Temperature Gradients on the Efficiency of Capillary Zone Electrophoresis Separations, Anal. Chem. 61, 241-246.

[4] Fletcher, P.D.I., Haswell, S.J., E., Pombo-Villar, Warrington, B.H., Watts, P., Wong, S., Zhang, X., 2002, Micro reactors: principles and applications in synthesis, TETRAHEDRON 58, 4735-4757.

[5] DeWitt, S., 1999, Microreactors for chemical synthesis, Combinational Chemistry 3, 350-356.

[6] Miyake, R., Lammerink, S.J., Elwenspoek, M., Fluitman, H.J., 1993, Micro mixer with fast diffusion, IEEE, 248-253.

[7] Bayraktar, T., Pidugu, S.B., 2006, Characterization of liquid flows in microfluidic systems, Int. J. of Heat and Mass Transfer 49, 815-824.

[8] Peng, X. F., Peterson, G. P., Wang, B. X., 1994, Frictional flow characteristics of water flowing through rectangular microchannels, Exp. Heat Transfer 7, 249–64.

[9] Xu, B., Ooi, k.T., Wong, N.T., 2000,Experimental investigation of flow friction for liquid flow in microchannels, Int. Comm. HeatMass Transfer 27, 1165-1176. Yovanovich, M.M., Advanced Heat Conduction, in preparation, Chapter 12.

[10] Ren, C.L., Li, D., 2003, Electroviscous effects on pressure-driven flow of dilute electrolyte solutions in small microchannels, J. Colloid and Interface Science 274, 319-330.

[11] Judy, J., Maynes, D., Webb, B.W., 2002, Characterization of frictional pressure drop for liquid flows through microchannels, Int. J. of Heat and Mass Transfer 45, 3477-3489.

[12] Tuckerman, D.B., Peace, R.F.W., 1981, High-Performance Heat Sinking for VLSI, IEEE ELECTRON DEVICE LETTERS EDL-2, 126-129.

[13] Mala, G. M., Li D., 1999, Flow characteristics of water in microtubes, nt. J. of Heat and Mass Transfer 20, 142-148.

[14] Pfhaler, J., Harley, J., Bau, H., 1990, Liquid transport in micron and submicron channels, Sensors Actuators A21–A23, 431–434.

[15] Pfhaler, J., Harley, J., Bau, H., Zemel, J. N., 1991, Gas and liquid flow in small channels Micromechnical sensors, actuators, and systems, DSC 32, 49–60.

[16] Urbanek, W., Zemel, J. N., Bau, H. H., 1993, An investigation of the temperature dependence of Poiseuille numbers in microchannel flow, J. Micromech. Microeng. 3, 206–208.

[17] Qu, W., Mala, G. M. and Li, D., 2000, Pressure-driven water flows in trapezoidal silicon microchannels, Int. J. Heat Mass Transfer 43, 353–364.

[18] Papautsky, I., Brazzle, J., Ameel, T., Frazier, A. B., 1999, Laminar fluid behavior in microchannels using micropolar fluid theory, Sensors Actuators 73, 101–108.

[19] Ren, C.L., Li, D., 2005, Improved understanding of the effect of electrical double layer on pressure-driven flow in microchannels, Analitica Chemica Acta 531, 15-23.

[20] Weilin, Q., Mala, H.M., Li, D., 2000,Pressure-driven water fows in trapezoidal silicon microchannels, Int. J. of Heat and Mass Transfer 43, 353-364.

[21] Guo, Z., Li, Z., 2003, Size effect on microscale single-phase flow and heat transfer, Int. J. of Heat and Mass Transfer 46, 149-159.

[22] Bahrami, M., Yovanovich, M.M., Culham, J.R., 2005, Pressure drop of laminar, fully developed flow in rough microtubes, ASME Journal of Fluids Engineering 128, 632-637.

[23] Jiang, X.N., Zhou, Z.Y., Huang, X.Y. , 1997, Liu, C.Y., Laminar flow through microchannels used for microscale cooling systems, in: IEEE/CPMT Electronic Packaging Technology Conference, 119-122.

[24] Baviere, R., Ayela, F., Le Person, S., Favre-Marinet, M., 2005, Experimental characterization of water flow through smooth rectangular microchannels, Physics of fluids 17.

[25] Bucci, A., Celata, G.P. , Cumo, M. , Serra, E., Zummo, G., 2003, Water single-phase fluid flow and heat transfer in capillary tubes, in: Int. Conference on Microchannels and Minichannels, Paper # 1037, ASME, vol. 1, 319–326.

[26] Wu, H.Y., Cheng, P., 2003, Friction factors in smooth trapezoidal silicon microchannels with different aspect ratios, Int. J. Heat Mass Transfer 46 , 2519–2525.

[27] Liu, D., Garimella, S., 2004, Investigation of liquid flow in microchannels, J. Thermophys. Heat Transfer, AIAA 18, 65–72.

[28] Gao, P., Le Person, S. , Favre-Marinet, M., 2002, Scale effects on hydrodynamics and heat transfer in two-dimensional mini and microchannels, Int. J. Therm. Sci. 41, 1017–1027.

[29] Steinke, M.E., Kandlikar, S.G., 2006, Single-phase liquid friction factors in microchannels, Int. J. Thermal Sciences 45, 1073-1083.

[30] Squires, T.M., Quake, S.R., 2005, Micro uidics: fluid physics at nanoliter scale, Review of modern physics 77, 977-1026.

[31] White, F. M., 1974, Viscous Fluid Flow, McGraw-Hill Inc., New York, Chapter 3.

[32] Shah, R.K., London, A.L., 1978, Laminar flow forced convection in ducts, *Supplement to advances in heat transfer*, Academic press, New York.

[33] Bahrami, M., Yovanovich, M.M., Culham, J.R., 2007, A novel solution for pressure drop in singly connected microchannels, Int. J. of Heat and Mass Transfer 50, 2492-2502.

[34] Timoshenko, S.P., Goodier, J.N. , 1970, Theory of Elasticity, McGraw-Hill Inc., New York,Chapter 10.

[35] Yovanovich, M.M., 1974, "A General Experesion for Predicting Conduction Shape Factors," AIAA, Thermophysics and Space Craft Control, Vol. 35, pp. 265-291.

[36] Yovanovich, M.M., 1974, "A General Experesion for Predicting Conduction Shape Factors," AIAA, Thermophysics and Space Craft Control 35, 265-291.

[37] Muzychka, Y.S. and Yovanovich, M.M., 2002, "Laminar flow friction and heat transfer in non-circular ducts and channels part 1: Hydrodynamic problem," Compact Heat Exchangers, A Festschrift on the 60th Birthday of Ramesh K. Shah, Grenoble, France, pp. 123–130.

[38] Erickson, D., Sinton, D., Li, D., 2003, Joule heating and heat transfer in poly(dimethylsiloxane) microfluidic systems, Lab-on-a Chip 3, 141-149.

[39] Holman, J.P., 2001, Experimental methods for engineering, 7th Ed., McGraw-Hill, New York, Chapter 3.

[40] Phillips, R.J., 1990, Microchannel heat sinks, *Advances in thermal modeling of electronic components and systems*, Hemisphere Publishing Corporation, New York, Chapter 3.

[41] Sharp, K.V., Adrian, R.J., Santiago, J.G., Molho, J.I., 2005, Liquid Flows in Microchannels, *MEMS Hand Book: Introduction and fundamentals*, 2nd Ed., Taylor & Francis Group, New York.

[42] Kandlikar, S.G., Garimella, S., Li, D., Colin, S., King, M.R., 2006, Heat transfer and fluid flow in minichannels and microchannels, Elsevier Limited, Oxford.

[43] Kays, W.M., London, A.L., 1984, Compact heat exchangers, McGraw-Hill, New York.

[44] Koo, J., Kleinstreuer, C., 2003, Liquid flow in microchannels: experimental observations and computational analyses of microfluidics effects, J. Micromech. Microeng. 13, 568-579.

[45] Probstein, R. F., 1994, Physicochemical Hydrodynamics, 2nd Ed., John Wiley & Sons.

[46] Masliyah, J.H., Bhattacharjee, S., 2006, Electrokicetic and colloid transport phenomena, JohnWiley & Sons, Inc., New Jersey.

[47] Lide, D., Kehiaian, H.V., 1994, CRC Handbook of Thermophysical and Thermochemical Data, 1st Ed., CRC Press, USA.

[48] Lee, J.S.H, Hu, Y., Li, D., 2005, Electrokinetick concentration gradient generation using a converging-diverging microchannel, Analytica Chemica Acta 543, 99-108.